

Large Hexosomes from Emulsion Droplets: Particle Shape and Mesostructure Control

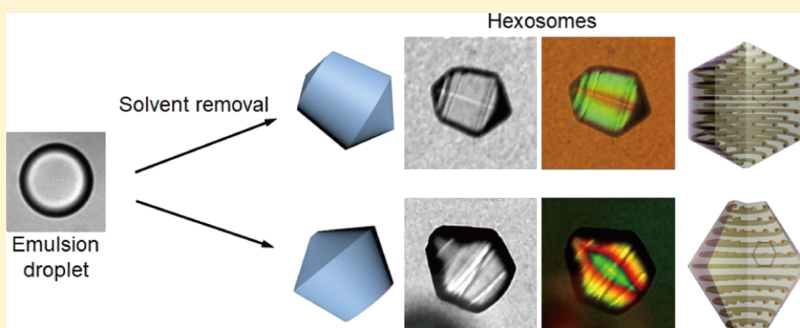
Haiqiao Wang,^{†,‡,§,||} Per B. Zetterlund,^{‡,§} Cyrille Boyer,^{‡,§} Ben J. Boyd,^{§,¶} Timothy J. Atherton,^{||} and Patrick T. Spicer^{*,†,‡,§,||}

[†]Complex Fluids Group, School of Chemical Engineering, and [‡]Centre for Advanced Macromolecular Design, School of Chemical Engineering, UNSW Sydney, Sydney 2052, Australia

[§]Monash Institute of Pharmaceutical Sciences, Monash University, Melbourne 3800, Australia

[¶]Department Physics and Astronomy, Tufts University, Boston 02155, Massachusetts, United States

Supporting Information



ABSTRACT: Soft, rotationally symmetric particles of dispersed hexagonal liquid crystalline phase are produced using a method previously developed for cubosome microparticle production. The technique forms hexosome particles via removal of ethanol from emulsion droplets containing monoolein, water, and one of the various hydrophobic molecules: vitamin E, hexadecane, oleic acid, cyclohexane, or divinylbenzene. The unique rotational symmetry of the particles is characterized by optical microscopy and small-angle X-ray scattering to link particle phase, shape, and structure to composition. Rheology of the soft particles can be varied independently of shape, enabling control of transport, deformation, and biological response by controlling composition and molecular structure of the additives. The direct observations of formation, and the resultant hexosome shapes, link the particle-scale and mesoscale properties of these novel self-assembled particles and broaden their applications. The micron-scale hexosomes provide a route to understanding the effects of particle size, crystallization rate, and rheology on the production of soft particles with liquid crystalline structure and unique shape and symmetry.

■ INTRODUCTION

Molecular self-assembly by amphiphilic materials such as block copolymers,¹ surfactants,² peptides,^{3,4} and lipids is a broadly applicable technology that enables active delivery⁵ as well as the creation of hierarchical structures⁶ and advanced materials.⁷ Liquid crystalline phases, for example, form spontaneously at moderate and high concentrations of amphiphiles in water and other polar solvents,⁸ and their underlying crystalline symmetry and mesostructure create a unique viscoelastic matrix⁹ that can solubilize hydrophobic, hydrophilic, and amphiphilic molecules to significant levels.¹⁰

Although bulk liquid crystalline materials are of interest for many applications, some uses require the self-assembled structures to be in a particulate form. Fortunately, a number of amphiphiles that form liquid crystals also have a low water solubility. The resultant two-phase coexistence that occurs at high dilutions¹¹ enables formation of dispersed nanostructured particles of liquid crystal¹² that can be sterically stabilized for wide use.^{13,14} Examples include dispersed lamellar phases, or

liposomes,¹⁵ fragmented bicontinuous cubic phases, or cubosomes,¹² and particles of hexagonal liquid crystalline phase, known as hexosomes.¹⁶

Nanostructured particles have biocompatible structures that are a key step in biological mechanisms such as digestion and nutrient delivery,¹⁷ holding much promise for controlled delivery of therapeutic molecules.¹⁸ Recent work on nanomedicine delivery¹⁹ and phagocytosis of particles²⁰ has highlighted the importance of nanoparticle and microparticle shape to the specificity and robustness of particle-based delivery methods. We seek to combine the benefits of particle shape with the enhanced performance of nanostructured materials, but the control of particle shape in liquid crystalline systems has not been studied in great detail. One reason for the lack of activity is the difficulty in direct observation of liquid

Received: August 3, 2018

Revised: October 12, 2018

Published: October 15, 2018

crystalline nanoparticles, as the observation of these objects requires cryo-transmission electron microscopy (cryo-TEM), studies that require expensive infrastructure and are inherently limited in the number of particles that can be studied. One solution is to increase the length scale of liquid crystalline particles, allowing study via simple optical microscopy methods and greatly increasing the versatility for observation.²¹

We recently showed the ability of micron-scale hexosomes to form a wide range of faceted soft particle shapes, depending on crystallization rate and the properties of solvent and additives.²¹ The ability to form such particles, using a simple emulsion precursor process,²² holds promise for controlled production of liquid crystalline particles with complex shapes, for example via microfluidics. The same approach should be feasible to study hexosome particles, provided the phase transition from cubic to hexagonal liquid crystalline phase can be incorporated into such a process. Hexosomes and hexagonal phase have been shown to be superior to bicontinuous cubic phase at inhibiting release of solubilized drugs,²³ and their inherent rotational symmetry offers a unique approach to form particle and colloid shapes with advantages in surface deposition and active matter.²⁴ Increased study and ease of use will be instrumental in expanding such applications.

Phase transition from cubic to hexagonal phase can be triggered by increasing temperature,^{2,25–27} adding hydrophobic molecules^{28–30} and changing pH.^{31,32} These conditions increase the effective volume of the hydrocarbon of the amphiphile, increasing the critical packing parameter and transforming the contorted bicontinuous amphiphile bilayers to hexagonally packed cylinders,²⁵ as shown in the schematic in Figure 1a. As a result, hexosomes can be made using the same mechanism that causes such phase transitions in bulk liquid crystals.

Hexosomes made in previous work were all nanoparticles,^{28,33–35} requiring specialized microscopy techniques for direct observation. Two-dimensional cryo-TEM³⁶ and atomic force microscopy³⁷ images suggest that hexosomes mainly form as either flat disklike hexagonal prisms (Figure 1b), or spherical shapes, but three-dimensional characterization is limited with such techniques.³⁸ Cryo-scanning electron microscopy (SEM) imaging³⁹ showed that some hexosomes can adopt a shape resembling a spinning top, a short cylinder capped at both ends by a cone, as shown in Figure 1c. Related biconical shapes with a central raised spine structure were also noted³⁹ and are shown as a schematic in Figure 1d, but multiple mesostructures have been proposed to explain the different shapes of particles with an underlying hexagonal symmetry.

Amphiphilic lipid hexosomes forming flat prisms were thought to form from hexagonally packed cylindrical micelles aligned perpendicular to the largest face.³⁶ Monoolein spinning top shapes were explained as cylinders aligned along their long axis,³⁹ similar to the proposed structure of unit cells in biconical single crystals of precipitated silicate.⁴⁰ Chromonic liquid crystal particles can also exhibit biconical shapes, despite having different rheology and building blocks from hexosomes, but were proposed to result from hexagonal columns curled around the central symmetry axis.⁴¹ Similar structures were directly observed in biconical block copolymer particles, with SEM images showing hexagonally packed cylinders wrapped around the central symmetry axis.⁴² Bulk hexagonal phase insights also help explain the ordering in hexosome particles. The radial confinement length scale, r , of hexagonal phase

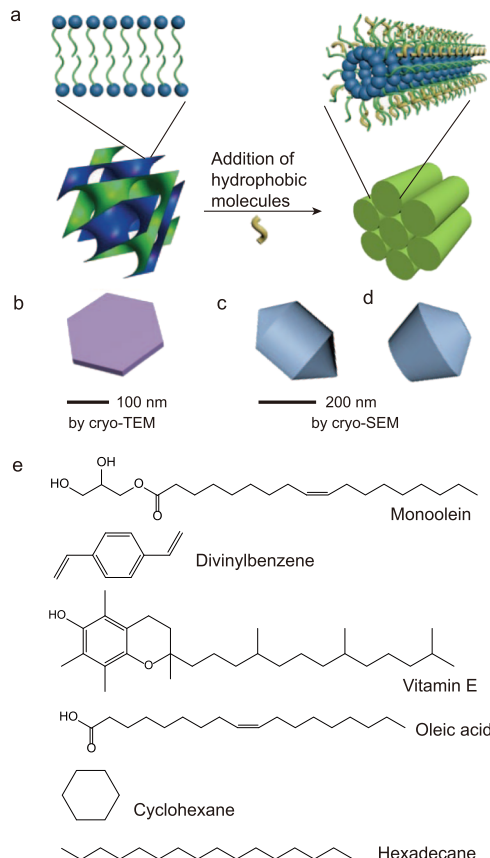


Figure 1. (a) Schematic of change in microstructure during transition from cubic to hexagonal phase; (b) hexosome shape and length scale observed by cryo-TEM;³⁶ (c) spinning top and (d) biconical shapes observed by cryo-SEM;³⁹ (e) molecular structure of the amphiphile and additive chemicals used in the formation of hexosomes.

structures in cylindrical capillaries was recently found to affect the transition between cylindrical micelles aligned with the mesostructure long axis, for $r > 0.2$ mm, and cylindrical micelles bent around the long axis, for $r < 0.2$ mm.⁴³

We are interested in more closely studying hexosome production above micron length scales to better understand how to control their shape and broaden applications. Larger hexosomes may also improve reservoir and controlled release properties, as the liquid crystalline phase diffusivity is too high for good performance of particles with nanoscale dimensions.⁴⁴ One promising route to using hexosomes as delivery vehicles is via enzymatic degradation of precursor emulsion droplets,^{26,45} so developing improved physical models of shape control will enable improvement and optimization of such applications.

Here, emulsion droplet precursors, containing ethanol and monoolein, are created, with varying amounts of either vitamin E, hexadecane, oleic acid, cyclohexane, or divinylbenzene (DVB) guest molecules⁴⁶ and dispersed into an aqueous continuous phase. The droplets transform into hexosomes following removal of ethanol,²¹ as confirmed by small-angle X-ray scattering (SAXS). The micron-scale hexosome particles tend to have underlying hexagonal symmetry,³⁹ though can exhibit significant variations in overall shape and proportions. Optical study indicates particle mesostructures are the cause of the shape variations and can be controlled by, for example, emulsion droplet size and levels of hydrophobic additives. The direct observations of formation, and the resultant hexosome

shapes, link the particle-scale and mesoscale properties of these novel self-assembled particles. Given the potential for soft particles to enable unique control of self-assembly and biological interactions, we are particularly motivated to understand the mechanisms by which the shapes and mechanical properties^{47–49} of such particles can be controlled in simple, scalable flow,²¹ and mixing processes.²²

MATERIALS AND METHODS

Commercial grade monoolein, Dimodan MO90K, was obtained from DuPont Danisco (Botany NSW, Australia). Ethanol (99%) and cyclohexane (99%) were purchased from Chem-Supply (Australia). Vitamin E (α -tocopherol, 96%), DVB (80%), hexadecane (99%), and oleic acid (90%, in the acid form at the pH of all hexosome samples) were purchased from Sigma-Aldrich (Castle Hill, NSW, Australia). Commercial vitamin E (Blackmores, Australia) was also used and contains structural isomers, unsaturated tocotrienols, and α -tocopherol.⁵⁰ Microfibrillated cellulose (MFC) was purchased from Wong Coco (Jakarta, Indonesia). All chemicals were used without further purification. Ultrapure water with a resistivity of 18.25 M Ω cm was obtained using a Sartorius ultrapure water purifier.

Hexosomes were formed by combination of a precursor solution and a diluting solution. All precursor solutions contained monoolein and ethanol with a weight ratio 1:1 and a desired amount of additives. The amount of additive is reported as a mass ratio of additive to monoolein. All experiments were carried out at 25 °C.

Initially, 0.02–0.2 mL of precursor was injected with a syringe into 3.5 mL of a diluting solution containing water, ethanol, and 0.1% w/w rheological modifier, MFC, that adds a yield stress to the fluid and allows three-dimensionally symmetric particle formation from droplets. The MFC is used only to immobilize the droplets and resultant particles, preventing coalescence and aggregation and enhancing microscopy accuracy. The cellulose fibers are much larger than the hexosome mesostructure, with fibers typically 5–10 μ m in length. As the pure cellulose material is insoluble in water, we see no effect on the phase behavior during control experiments, in agreement with our previous work that found no structural changes caused by MFC during cubosome formation.²¹ The ethanol concentration in the diluting solution was 25% v/v. Mixing the two solutions forms emulsion droplets that are then transformed into hexosomes by evaporation of ethanol from the suspension at a rate of 2.3 mg/min. These concentrations provided both the necessary driving force magnitude and a sufficiently slow rate to produce well-formed particles, as we found in our previous work on cubosome formation.²¹

All particle formation experiments were carried out with samples in an open Petri dish with a liquid height of 4 mm and a free surface area of 9.6 cm² to facilitate evaporation of ethanol and induce liquid crystal formation. The sample was held at constant $T = 25$ °C and relative humidity = 60% in a static environment during the transition process from droplets to particles. Time-dependent microscopic observations were performed by sampling from the Petri dish containing the suspension. Once the desired shapes were formed, the suspending yield stress matrix was diluted to allow easy particle recovery.

Microscopy observations were conducted on a Leica DM2500M optical microscope with a Leica N PLAN 10X EPI objective lens 10/0.25, and all images were recorded using a Moticam 10 MP digital camera. Micrographs shown here portray shapes representative of dispersions of more than 100 particles in a sample, and all image analysis of shape was performed using ImageJ.⁵¹ Polarizing microscopy texture analysis is a primary tool for studying liquid crystalline phases that are optically anisotropic and birefringent. The liquid crystals can split an incoming light beam into two components, one of which can pass through an analyzer that is crossed relative to the polarizer, making the sample appear bright. Transmitted light intensity changes with sample orientation relative to the polarizer and the colorful patterns indicate interference of the split light.⁵² In the hexagonal phase, specific birefringence textures indicate certain molecular packing and defects of microstructure.^{53,54}

Synchrotron SAXS was used to identify the liquid crystalline structures responsible for larger-scale symmetry and faceting of all particles produced here. Samples were sealed into flat quartz cells mounted vertically on a remotely operated X–Y–Z translation stage at a temperature of about 25 °C at the Australian Synchrotron SAXS/wide-angle X-ray scattering beamline⁵⁵ and exposed to an X-ray beam with a wavelength of 1.12 Å, energy 11 keV, with a sample-to-detector distance of 1034 mm. The setup provides a q range from $0.018 < q < 1.02 \text{ \AA}^{-1}$, where q is the magnitude of the scattering vector, defined as $q = 4\pi/\lambda \sin(\theta/2)$, λ is the radiation wavelength, and θ is the scattering angle. Two-dimensional, spatially resolved SAXS patterns were collected using 100 μ m steps on the translation stage, with a 1 s acquisition at each position. A Pilatus 1 M detector with an active area of $169 \times 179 \text{ mm}^2$, and a pixel size of 172 μ m, was used for acquisition. The two-dimensional SAXS patterns were then integrated into a one-dimensional scattering function $I(q)$ using ScatterBrain Analysis software.⁵⁶ The phase type is identified by correlating q values of the peaks with Miller indices (hkl) for known liquid crystalline phases, and the ratio $\sqrt{1} : \sqrt{3} : \sqrt{4}$ corresponds to hexagonal phase ($p6mm$). Lattice parameters, a , the repeat distance of the microstructure, are calculated using the equation $a = 4\pi\sqrt{h^2 + k^2 + hk / \sqrt{3}q_{hk}}$.⁵⁷

Rheological characterization of bulk liquid crystalline phases was performed using a DHR-1 rheometer from TA Instruments using an oscillatory stress sweep at a constant frequency of 1 Hz. A 40 mm cone and plate geometry with 2 degree angle was used for all measurements and a solvent trap was used to avoid evaporative losses. Elastic modulus is measured as the plateau value attained at low stresses in the linear viscoelastic regime.

RESULTS AND DISCUSSION

Micron-scale hexosomes were made using a previously developed droplet precursor method,²¹ with the addition of various hydrophobic additives, vitamin E, DVB, hexadecane, and oleic acid (Figure 1e), that ensure formation of inverse hexagonal liquid crystalline phase. Emulsion droplets are formed by dispersion of the precursor solution into an aqueous yield stress continuous phase, trapping the droplets and enabling their three-dimensional transformation into liquid crystalline particles. Figure 2a,b shows optical microscopy

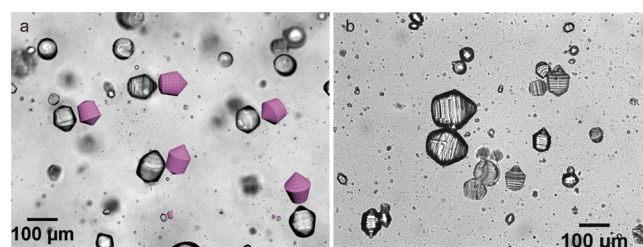


Figure 2. (a) Optical micrograph of multiple hexosomes formed using the droplet precursor method along with drawn three-dimensional representations of the particle shapes. (b) Details of the circular ridges formed on some hexosomes are visible here, aiding in visualizing their three-dimensional forms.

images of polydisperse hexosomes formed by this method. The particles have a wide size range that is set by the starting precursor emulsion droplet size distribution, allowing hexosomes to be produced with diameters from at least 1–100 μ m. Three-dimensional drawings are also included in Figure 2a, indicating the types of shapes formed during the droplet phase transition. In all of our experiments, we typically see a mixture of both spinning top and bicone shapes. The evolution of these shapes as ethanol is removed is the result of

the phase transition from isotropic droplets to hexagonal liquid crystalline phase.

The transition process from droplet to hexosome is shown in Figure 3, with adjacent brightfield and polarized light images

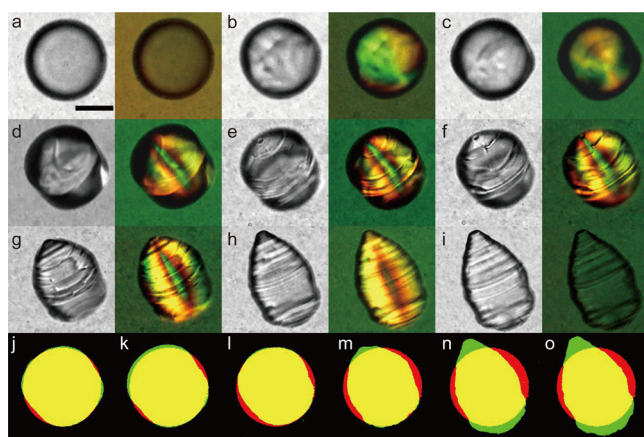


Figure 3. Transition process from droplet to hexosome for an initial weight ratio of DVB to monoolein $n_{\text{DVB}} = 0.6$: (a) 36, (b) 63, (c) 66, (d) 76, (e) 138, (f) 186, (g) 263, (h) 381, and (i) 520 min; the left image is under bright field and the right is under polarized light; comparison of droplet precursor with particles formed at (j) 66, (k) 76, (l) 186, (m) 263, (n) 381, and (o) 520 min from left to right; particles are shown in green, droplet precursor is in red, and the overlapping part is in yellow. Hydrophobic molecule is DVB. Scale bar is $50 \mu\text{m}$.

indicating, respectively, shape and structural change. The initial emulsion droplet is spherical and isotropic under polarized light, as it is unstructured and interfacial tension dominates droplet rheology in determination of shape. In Figure 3b, 63 min after the droplet precursor is made, the appearance of birefringence indicates that the hexagonal phase starts to form, and the shape shows a small change to a more anisotropic form. As ethanol continues to evaporate, vertices grow and become sharper with time, and birefringence becomes more intense, indicating that an increasingly ordered microstructure is crystallizing.⁵⁸ After about 3 h elapsed time, the shape now has striking rotational symmetry about a clearly visible central axis core, as shown in Figure 3a–f. As growth continues, the surface becomes more non-uniform as the particle rheology becomes increasingly elastic, but the circular ridges visible indicate that the particle maintains rotational symmetry. The hexosomes in Figure 3 are not entirely consistent with past observations of nanoscale hexosomes, which are flat disklike hexagonal prisms, Figure 1b, or spherical shapes, but are similar to the spinning top shape with a spine observed via cryo-SEM (Figure 1c,d).³⁹ The larger-scale hexosomes made here are more easily observed from different orientations via optical microscopy because of their larger size, providing additional information to electron microscopy studies.

After forming their initial shape from the precursor droplets, the hexosomes continue to change shape but their longer axis is still smaller than the diameter of the initial precursors, as shown in the comparison in Figure 3j–l. The droplet volume decreases as ethanol diffuses from the droplet to the continuous phase, and the volume of droplet as a function of time is calculated from the microscopy images in Figure 3 and plotted in Figure S1. During the first 76 min, the decrease in volume is small, so it is not obvious in Figure 3j–l. After that,

the volume decreases more significantly. At longer times, Figure 3g–i, the particle grows longer along the symmetry axis, increasing particle aspect ratio with time and decreasing the angle at the conical apex. Comparing shapes at longer times in Figure 3m–o with the droplet precursor, the hexosome grows outside the initial precursor boundary at both ends of the central axis, while the diameter perpendicular to the long axis decreases. Figure S1 shows a decrease in the volume of particle from about 5 h.

Shape evolution of the hexosomes can continue if the hydrophobic additive molecules are permitted to diffuse out of the particles along with the ethanol. In Figure 3, DVB is more soluble in the surrounding aqueous environment and more volatile than the monoolein, enabling it to leave the particle and eventually evaporate, consistent with past work on loss of volatile solubilized additives from liquid crystals.⁵⁹ At long times, most of the DVB is lost, as is the initial liquid crystalline phase of the hexosomes, indicated by the disappearance of the particle birefringence in the polarized light images in Figure 3g–i. In Figure 3i, the particle has transformed into a bicontinuous cubic phase after significant loss of the hydrophobic molecule additive to attain or fall below the phase boundary at $n_{\text{DVB}} = 0.04$. The increased volume may be the result of water entering the particle and further swelling the phase, Figure S1. Growth of large hexosomes from droplets is a way to create particles with unique shapes, and a central aspect of the process is particle mesostructure and its control by additive levels.

Figure 4a–c examines the shape, using microscopy images, and structure, using SAXS, of hexosomes formed at different initial weight ratios of DVB to monoolein, n_{DVB} . All particles possess a partial or complete hexagonal liquid crystalline structure, as seen in Figure 4a–c. Additional microscopy images of particles with the same n_{DVB} are shown in Figure S2. For the two extreme DVB levels, the birefringence is markedly different to the ordered middle example, indicating that although the system is mostly hexagonal and anisotropic, the hexagonal regions are slightly disordered or multidomain. In contrast, the middle example is highly symmetric in its color arrangement and likely an example of a monodomain of hexagonal phase. When $n_{\text{DVB}} = 0.2$, Figure 4a, microscopy indicates that the particles are nonspherical, with rounded corners and wrinkles at their surfaces, indicative of a biconical shape but without the distinct rotational symmetry seen in Figure 3e–h. However, the birefringence shown by the particle, and the SAXS result in Figure 4a, both indicate the formation of hexagonal phase at this composition.

A partial phase diagram of DVB–monoolein with different weight ratios of water and ethanol is shown in Figure 4d, mapping the range of compositions over which the hexosome particles can stably form. Although we focus here on the formation of particles by a kinetic process of solvent removal, the particles shown are often not the final, long-time state of the system. Simulations have shown, however, that the full equilibrium sequence of phase transitions is observed in such processes, so we expect the phase diagrams to be of use in describing the process.⁶⁰ During the transition from emulsion droplets to hexosomes, the process is represented by a path from the point of initial concentration to the hexosome region, moving toward the lower left of the phase diagram, as ethanol and DVB both leave the system and their concentrations decrease. At a low n_{DVB} of 0.2, ethanol can change the system from hexagonal (H_2) to cubic phase (Q_2). When $n_{\text{DVB}} = 0.2$, in

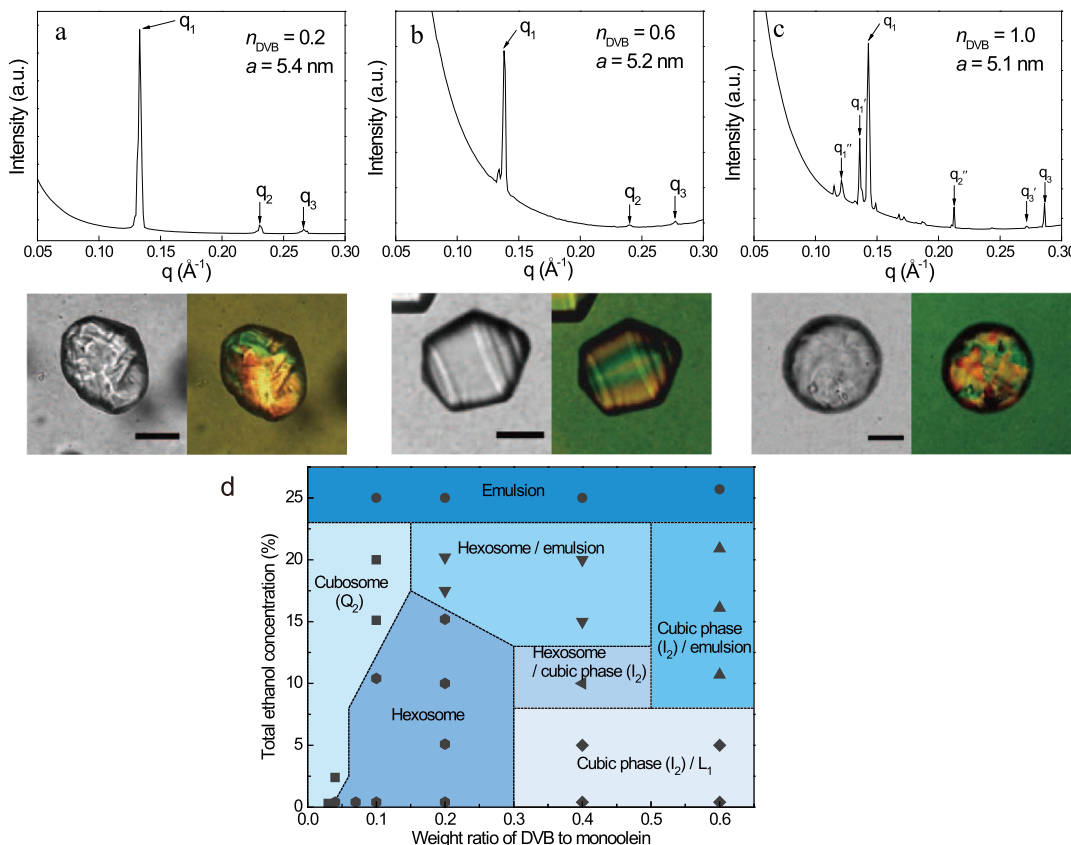


Figure 4. SAXS and microscopy images of hexosomes with different levels of DVB additive, taken 5 h after initial droplet formation. The precursor solutions contain $n_{\text{DVB}} =$ (a) 0.2, (b) 0.6, and (c) 1. The left image is under bright field and the right is under polarized light. Scale bar is 50 μm . (d) Partial phase diagram of the DVB–monoolein–ethanol–water system with different weight ratios of DVB to monoolein and varying concentrations of ethanol.

the transition from emulsion droplets to particles, the composition passes through a cubic phase region and then goes down to hexagonal phase. Therefore, cubosomes may form at an early stage of the transition and then transform to hexosomes. These cubosomes are unnoticed during our observations, possibly because they are not birefringent and only exist for a short time. However, as cubosomes are in a different symmetry and have higher elasticity, their formation can affect the final particle shape, influencing formation of the hexosomes with disordered shapes in Figure 4a. At ratios of DVB higher than 0.5, the phase changes from hexagonal to micellar cubic phase (I_2). For a starting ratio of $n_{\text{DVB}} = 1.0$, the trajectory passes through the micellar cubic phase region at an early stage of transition. The formation of cubic phase in the process also results in the disordered shape in Figure 4c. For the initial ratio of $n_{\text{DVB}} = 0.6$, no other liquid crystal phase forms before the hexagonal phase, and the particle shape in Figure 4b shows clear hexagonal phase symmetry.

Another possible reason for the irregular shape in Figure 4a is that the microstructure of cylindrical micelles cannot pack in an orderly fashion over distances greater than several tens of microns, which is important for the formation of ordered particle shapes.⁴¹ The addition of hydrophobic additives can induce the formation of inverse hexagonal phase by lowering the packing frustration energy of the amphiphile hydrocarbon chains. At a small concentration of hydrophobic additive, for example, $n_{\text{DVB}} = 0.2$, hexagonally packed cylindrical micelles can have void space between them, requiring hydrocarbon chains to stretch or compress to avoid the empty space,

especially at large lattice parameters.⁶¹ More disordered domain arrangements and greater numbers of defects can then result, as seen in the polarized light image in Figure 4a, despite the overall uniformity of hexagonal phase formation. Additional hydrophobic molecules can further decrease the packing frustration energy by filling the void space between cylinders and increasing the hydrophobic moiety.⁶¹ The inverse interfacial curvature is also increased, reducing the lattice parameter, as we see moving from Figure 4a–c in the SAXS data.

Hexosome particles formed at a larger $n_{\text{DVB}} = 0.6$, Figure 4b, exhibit clear spinning top shapes, with a strongly symmetric birefringence pattern that the SAXS result in Figure 4b confirms is due to the formation of hexagonal phase. When $n_{\text{DVB}} = 0.6$, particle shapes are rotationally symmetric with a clear order to the birefringent color arrangements in the polarized light image. The improved shape and structure result from increased flexibility of the cylindrical micelles in the mesostructure, allowing them to bend and form the rotationally symmetric structures with a lower energetic penalty.

When n_{DVB} increases to 1, the particle shapes lose their symmetry, becoming more spherical, but remain birefringent, Figure 4c. The SAXS data in Figure 4c show mixed hexagonal phases with different lattice parameters, and weak peaks that may indicate the presence of a micellar cubic phase I_2 . The I_2 phase can form above certain levels of hydrophobic additives in the hexagonal phase,²³ indicating a less-ordered polycrystalline microstructure that preferentially forms a spherical particle shape. Other hydrophobic additive molecules can also be

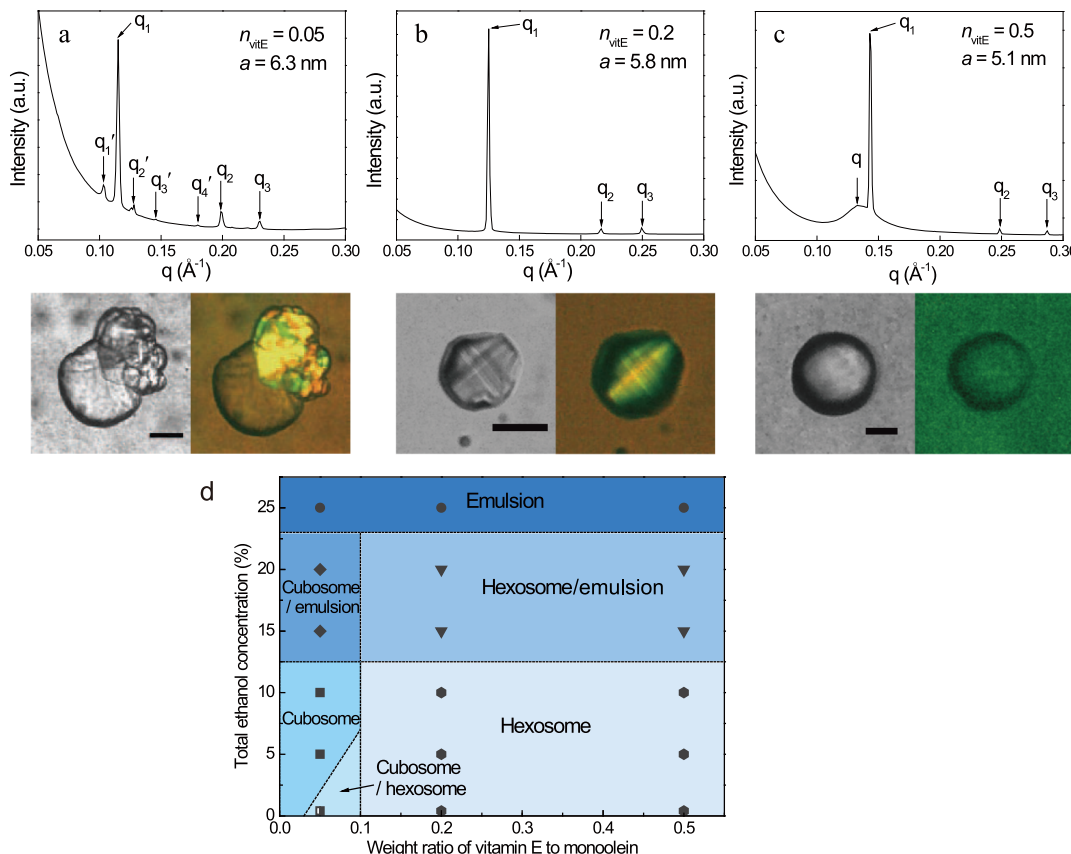


Figure 5. SAXS and microscopy images of hexosomes with addition of vitamin E. The weight ratio of vitamin E to monoolein is n_{VitE} = (a) 0.05, (b) 0.2, and (c) 0.5; the left image is under bright field and the right is under polarized light. Scale bar is 50 μm . (d) Partial phase diagram of the vitamin E–monoolein–ethanol–water system with different weight ratios of vitamin E to monoolein and varying concentrations of ethanol in excess solvent.

accommodated in particles and form hexosomes, broadening applications from synthetic polymeric materials, for example, to food and pharmaceutical components.

The hydrophobic molecule vitamin E acetate was found to form bulk hexagonal phase and nanoparticle hexosomes in previous studies,³⁰ and we use vitamin E in a similar way here to induce hexosome formation in microscale monoolein emulsions. Figure 5a–c shows microscopy images of particles containing different amounts of vitamin E in brightfield and polarized light, and the corresponding SAXS data indicate the packing of the lipid domains of the particles. More microscopy images of particles with the same n_{VitE} are shown in Figure S3. When the weight ratio of vitamin E to monoolein is $n_{\text{VitE}} = 0.05$, biphasic cubosome–hexosome structures form, Figure 5a, with isotropic and birefringent regions such as the nanoscale “Janus” particles observed by others using cryo-TEM.⁶² Scattering peaks of hexagonal phase, indicated by peak spacing ratios of 1, $\sqrt{3}$, and 2, and $Pn3m$ cubic phase, with peak spacing ratios of $\sqrt{2}$, $\sqrt{3}$, and 2, are both found, identified as q and q' in Figure 5a respectively.

When more vitamin E is added ($n_{\text{VitE}} = 0.2$), biconical hexosomes with strong birefringence form, as shown in Figure 5b. The shape is similar to the spinning top structure with a raised spine observed by cryo-SEM.³⁹ SAXS results display the three peaks of hexagonal phase, Figure 5b, demonstrating again the ability of the hexagonal phase to form particles with unique rotational symmetry. Upon increasing n_{VitE} to 0.5, particles lose their nonspherical shape and the birefringence becomes weak,

Figure 5c, and the SAXS result shows mixed phases are present. In Figure 5c, a wide peak q is visible along with a hexagonal phase, peaks q_1 , q_2 , and q_3 , which indicates an isotropic phase that dominates the particle behavior.^{28,29} The lattice parameter of hexagonal phase, a , calculated from SAXS data shows that it decreases with n_{VitE} from 6.3 nm when n_{VitE} is 0.05, to 5.8 nm when n_{VitE} is 0.2, and to 5.1 nm when n_{VitE} is 0.5. Vitamin E has a different type of effect from DVB on the molecular packing in the liquid crystal phase, as its hydroxyl group allows it to be partially hydrated and reduces the level of monoolein hydration.⁶³

A phase diagram is plotted for the vitamin E system in Figure 5d. Particle formation from the initial droplets occurs by movement from the initial composition straight down vertically, as the ratio n_{VitE} is unchanged with loss of ethanol. Similar to the DVB system, cubic phases are present at low ratios of vitamin E to monoolein, below $n_{\text{VitE}} = 0.05$, which causes “Janus” particle formation. When n_{VitE} increases to 0.2 and 0.5, the phase and particle shapes are consistent, and the particle formation trajectory has no effect on the resulting shapes.

Figure 6 shows a summary of the plateau elastic modulus of several different hexagonal phase liquid crystals along with a microscopy image of a typical hexosome formed at that composition. When hexosomes form, similar to bulk hexagonal phase,⁶⁴ their rheology can vary dramatically. All, however, have sufficient elasticity to resist interfacial tension and maintain a nonspherical shape.^{65,66} The values of elastic

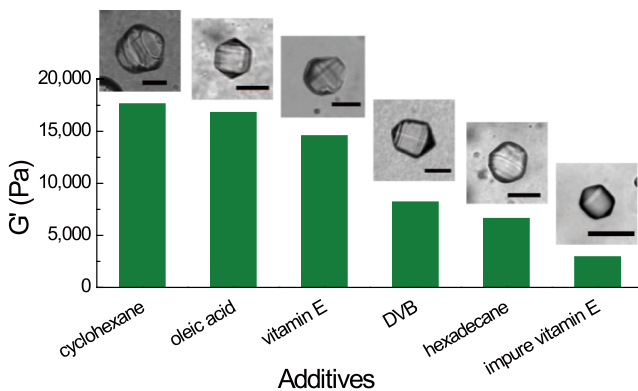


Figure 6. Plot of the plateau elastic modulus of bulk hexagonal phase for several hydrophobic additives with the same ratio to monolein, $n_{\text{additive}} = 0.2$. Microscopy images are hexosomes with the same composition as bulk phase. Modulus varies by more than 1 order of magnitude, but the rotationally symmetric shape remains stable for all cases. Scale bar is $50 \mu\text{m}$.

modulus in Figure 6 show that the bulk hexagonal phase ranges from 10^3 to 10^4 Pa with a yield stress between 100 and 600 Pa. The Laplace pressure, which drives less solidlike structures back into a spherical shape, is estimated to range from 2 to 200 Pa for particles on the order of $100 \mu\text{m}$ and an interfacial tension in the range of 0.1–10 mN/m.^{67,68} An important result of Figure 6 is that the elasticity of hexagonal phase can be varied by more than an order of magnitude by including different additive molecules, but it has no effect on the rotationally symmetric shape of hexosomes. It is therefore more likely that the packing of the mesostructure is the crucial determining factor in the shape of a micron-scale hexosome. Besides preserving a nonspherical shape, the elasticity of the hexosome particles is also useful for preserving a record of the growth process. We can infer possible details about the growth of the liquid crystal-isotropic phase boundary by observing the tracks of growth recorded inside the hexosomes.

Figure 7 shows close-up optical microscopy images of a hexosome formed from vitamin E at a weight ratio of $n_{\text{VitE}} = 0.3$, where a clear spiral structure is visible at the particle center. On the basis of past observations in viscoelastic liquid crystalline phases,^{21,69} we speculate that the structure is a region of isotropic micellar phase liquid, L_1 , enclosed within the hexagonal phase. A similar effect was seen for polyhedral particles of cubic phase, though the L_1 phase inclusions in $Pn3m$ crystals are faceted shapes inside the larger polyhedral shapes of the overall particle²¹ and can be induced by controlling the crystallization rate.^{70,71} Spiral defects are also observed in biomolecular and inorganic solid crystals, indicating the arrangement of repeating units.^{72,73} The L_1 inclusion forms because phase separation occurs during the transition process from isotropic emulsion droplets to

hexosomes. Some of the water and ethanol accumulates inside the particle and forms L_1 phase and is more likely to form in larger particles because of slower diffusion. The L_1 inclusion demonstrates that the hexosomes are mostly full of elastic liquid crystal phase and are not hollow or liquid-filled. Additionally, the spiral L_1 inclusion, as well as the circular lines visible at the surface of hexosomes, Figure 4, indicates the rotational trajectory of droplet crystallization, which is helpful to understand how the microstructure and cylindrical micelle packing evolves with time.

Past work indicates the bulk hexagonal phase can form two configurations, straight and ringed cylinders, depending on the length scale of confinement, with ringed cylinders forming at length scale $r < 200 \mu\text{m}$.⁴³ At larger characteristic length scales, straight cylinders can form that are parallel to the capillary axis.⁴³ The reason for the size effect is that undulation occurs in straight and parallel cylindrical micelles as a result of thermomechanical instability.^{74,75} Therefore, a hexagonal phase confined to a length scale smaller than the undulation range interferes with the stability of straight cylinder packing. Deformations are common in single phase domains, and bending of cylinders is the easiest one that occurs in the hexagonal phase as the resulting increase in elastic strain energy is lower than for other deformations, such as splay or twist. Curved hexagonally packed cylindrical micelles are frequently observed in inverse hexagonal phase domains,⁶⁷ and it is likely here that a closed rotating cylinder configuration is the most stable packing for some range of the length scales examined in our droplet studies. When larger than a size of about $200 \mu\text{m}$, all the particles possess irregular shapes, as there is no driving force for the rotationally oriented packing to form. Instead, multidomain hexagonal phases form and can yield disordered particle shapes.

At much smaller length scales, on the order of nanometers, another critical size appears for the concentric and rotating configuration.⁷⁶ At such high curvatures, the high bending energy of rotating cylinders prevents their formation, so parallel straight cylinders dominate because of the higher stability. This likely explains why a defect core line forms in the middle of a hexosome, as visible in Figures 3e,f and 8a,b, and also observed in other works.^{41,43,76} The limited optical resolution of our observations indicates that the diameter of the core lines seen here is smaller than $1 \mu\text{m}$ and is a function of the stiffness of cylindrical micelles and their crystallization rate. The core size measured for confined bulk phases⁴³ is much larger than the core we see here, indicating that the droplet formation of hexosomes is advantageous for creating different length scale particle structures with clear hexagonal monodomains.

Hexosomes made in this work match the birefringence patterns of bulk hexagonal phase arranged as cylinders wrapped around a central long axis.⁴³ As Figure 8a shows,

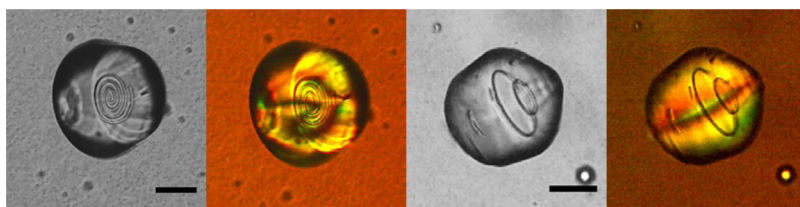


Figure 7. Microscopy image of hexosomes formed at $n_{\text{VitE}} = 0.3$, with a spiral L_1 phase inclusion inside. Scale bar is $50 \mu\text{m}$.

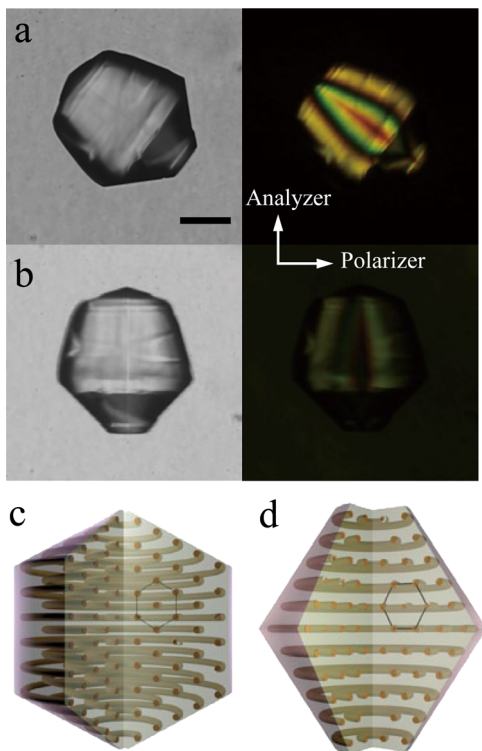


Figure 8. Microscopy image of hexosome particle in brightfield (left) and polarized (right) light, when the orientations of a polarizer and an analyzer are perpendicular to each other: (a) particle locates at a 45° angle to the direction of polarized light from the polarizer; (b) particle is parallel to the direction of polarized light from the polarizer. Scale bar is $50\ \mu\text{m}$. (c,d) Schematic of two types of hexosome microstructures. The yellow cylinders indicate the cylindrical micelles. The black hexagons depict the 2D hexagonal ordering of cylinders in the cross section.

when the symmetry axis of a hexosome is oriented 45° to the polarizer, a bright, colorful, and symmetric pattern is observed, indicating symmetric arrangement of the cylindrical micelles around the central axis.⁴³ Also consistent with bulk ringed cylinder results, when the particle is rotated parallel to the polarizer orientation, Figure 8b shows that the intensity weakens significantly, indicating that these hexosomes have a structure represented by the schematics in Figure 8c,d. Different orientations of the hexagonally packed cylinders can lead to further complexity, as the experimentally observed hexosomes often show imperfect shapes versus the shapes drawn in Figure 8c,b, and we commonly observe cases where asymmetric cone angles appear. This is likely due to different rates of ordering and formation during transition within the droplets, as well as other defects that can form in bulk hexagonal phases.^{67,77} We speculate that nanoparticle hexosomes also have a rotational packing when forming a spinning top shape, like the larger ones we produce here, in agreement with EM studies of block copolymer systems,⁴² but more work is needed. Of the other shapes formed in nanoparticle studies, we do not observe formation of flat hexagonal prisms, although it might be possible to produce more two-dimensional shapes using, for example, thin film forms of precursor droplets. As nanoscale hexosomes are made by the “top-down” method, in which particles form via fragmentation of bulk hexagonal phase, multiple conditions could affect shapes and microstructures, such as energy input

and temperature. More studies are needed to explain the variations in microstructures and improve control over packing and particle shape.

CONCLUSIONS

This work demonstrates a new method to produce hexosome particles, using a simple emulsion precursor process, that enables careful study of structure and shape development during liquid crystal formation. Similar to an earlier work on cubic liquid crystalline phases,²¹ this system forms the hexagonal phase by the removal of solvent from isotropic droplets suspended in a low-viscosity yield stress fluid that allows formation of soft particles without external surface or interfacial effects. The micron-scale hexosomes predominantly form shapes with rotational symmetry, evoking one of several shapes formed by nanoparticle hexosomes. Study of the larger hexosomes indicates that a significant degree of control over final particle shape could be attained using experimental variables such as droplet size, crystallization rate, and surfactant packing parameter. The findings of this work can be used, to some extent, to explain past work on nanoparticle shape formation, though the lower boundaries of length scale found here match the upper extremes of nanoparticle hexosome sizes previously studied. Planned future work includes using these soft particles as templates for hard particle synthesis in order to explore hierarchical self-assembly⁷⁸ by the unique symmetries.

ASSOCIATED CONTENT

S Supporting Information

The Supporting Information is available free of charge on the ACS Publications website at DOI: [10.1021/acs.langmuir.8b02638](https://doi.org/10.1021/acs.langmuir.8b02638).

Change of particle volume as a function of time during the transition process; additional microscopy images of hexosomes with different levels of DVB additive; and additional microscopy images of hexosomes with different levels of vitamin E additive ([PDF](#))

AUTHOR INFORMATION

Corresponding Author

*E-mail: p.spicer@unsw.edu.au.

ORCID

Haiqiao Wang: [0000-0002-7938-6422](#)

Per B. Zetterlund: [0000-0003-3149-4464](#)

Cyrille Boyer: [0000-0002-4564-4702](#)

Ben J. Boyd: [0000-0001-5434-590X](#)

Patrick T. Spicer: [0000-0002-8562-3906](#)

Notes

The authors declare no competing financial interest.

ACKNOWLEDGMENTS

The authors thank Dr. Marco Caggioni (Procter & Gamble Company, USA) for discussions of particle birefringence and structure relationships. TJA acknowledges support from National Science Foundation Grant No. DMR-1654283.

REFERENCES

- (1) Mai, Y.; Eisenberg, A. Self-assembly of block copolymers. *Chem. Soc. Rev.* **2012**, *41*, 5969–5985.
- (2) Gong, X.; Moghaddam, M. J.; Sagnella, S. M.; Conn, C. E.; Danon, S. J.; Waddington, L. J.; Drummond, C. J. Lyotropic Liquid

- Crystalline Self-Assembly Material Behavior and Nanoparticulate Dispersions of a Phytanyl Pro-Drug Analogue of Capecitabine—A Chemotherapy Agent. *ACS Appl. Mater. Interfaces* **2011**, *3*, 1552–1561.
- (3) De Santis, E.; Ryadnov, M. G. Peptide self-assembly for nanomaterials: The old new kid on the block. *Chem. Soc. Rev.* **2015**, *44*, 8288–8300.
- (4) Mandal, D.; Nasrolahi Shirazi, A.; Parang, K. Self-assembly of peptides to nanostructures. *Org. Biomol. Chem.* **2014**, *12*, 3544–3561.
- (5) Rizwan, S. B.; Boyd, B. J.; Rades, T.; Hook, S. Bicontinuous cubic liquid crystals as sustained delivery systems for peptides and proteins. *Expert Opin. Drug Delivery* **2010**, *7*, 1133–1144.
- (6) Carroll, N. J.; Rathod, S. B.; Derbins, E.; Mendez, S.; Weitz, D. A.; Petsev, D. N. Droplet-Based Microfluidics for Emulsion and Solvent Evaporation Synthesis of Monodisperse Mesoporous Silica Microspheres. *Langmuir* **2008**, *24*, 658–661.
- (7) Kresge, C. T.; Leonowicz, M. E.; Roth, W. J.; Vartuli, J. C.; Beck, J. S. Ordered mesoporous molecular sieves synthesized by a liquid-crystal template mechanism. *Nature* **1992**, *359*, 710–712.
- (8) Laughlin, R. G. *The Aqueous Phase Behavior of Surfactants*; Academic Press: London, 1995; p 200.
- (9) Mezzenga, R.; Meyer, C.; Servais, C.; Romoscanu, A. I.; Sagalowicz, L.; Hayward, R. C. Shear Rheology of Lyotropic Liquid Crystals: A Case Study. *Langmuir* **2005**, *21*, 3322–3333.
- (10) Drummond, C. J.; Fong, C. Surfactant Self-Assembly Objects as Novel Drug Delivery Vehicles. *Curr. Opin. Colloid Interface Sci.* **2000**, *4*, 449–456.
- (11) Spicer, P. *Encyclopedia of Nanoscience and Nanotechnology*; Marcel Dekker: New York, 2004; pp 881–892.
- (12) Gustafsson, J.; Ljusberg-Wahren, H.; Almgren, M.; Larsson, K. Cubic Lipid–Water Phase Dispersed into Submicron Particles. *Langmuir* **1996**, *12*, 4611–4613.
- (13) Chong, J. Y. T.; Mulet, X.; Waddington, L. J.; Boyd, B. J.; Drummond, C. J. High-Throughput Discovery of Novel Steric Stabilizers for Cubic Lyotropic Liquid Crystal Nanoparticle Dispersions. *Langmuir* **2012**, *28*, 9223–9232.
- (14) Chong, J. Y. T.; Mulet, X.; Keddie, D. J.; Waddington, L.; Mudie, S. T.; Boyd, B. J.; Drummond, C. J. Novel Steric Stabilizers for Lyotropic Liquid Crystalline Nanoparticles: PEGylated-Phytanyl Copolymers. *Langmuir* **2014**, *31*, 2615–2629.
- (15) Almgren, M.; Edwards, K.; Karlsson, G. Cryo transmission electron microscopy of liposomes and related structures. *Colloids Surf., A* **2000**, *174*, 3–21.
- (16) Larsson, K. Aqueous dispersions of cubic lipid–water phases. *Curr. Opin. Colloid Interface Sci.* **2000**, *5*, 64–69.
- (17) Fong, W. K.; Salentinig, S.; Prestidge, C. A.; Mezzenga, R.; Hawley, A.; Boyd, B. J. Generation of Geometrically Ordered Lipid-Based Liquid-Crystalline Nanoparticles Using Biologically Relevant Enzymatic Processing. *Langmuir* **2014**, *30*, 5373–5377.
- (18) Phan, S.; Salentinig, S.; Prestidge, C. A.; Boyd, B. J. Self-assembled structures formed during lipid digestion: characterization and implications for oral lipid-based drug delivery systems. *Drug Delivery Transl. Res.* **2013**, *4*, 275–294.
- (19) Hinde, E.; Thammasiraphop, K.; Duong, H. T. T.; Yeow, J.; Karagoz, B.; Boyer, C.; Gooding, J. J.; Gaus, K. Pair correlation microscopy reveals the role of nanoparticle shape in intracellular transport and site of drug release. *Nat. Nanotechnol.* **2016**, *12*, 81–89.
- (20) Champion, J. A.; Mitragotri, S. Role of target geometry in phagocytosis. *Proc. Natl. Acad. Sci. U.S.A.* **2006**, *103*, 4930–4934.
- (21) Wang, H.; Zetterlund, P. B.; Boyer, C.; Boyd, B. J.; Prescott, S. W.; Spicer, P. T. Soft polyhedral particles based on cubic liquid crystalline emulsion droplets. *Soft Matter* **2017**, *13*, 8492–8501.
- (22) Spicer, P. T.; Hayden, K. L.; Lynch, M. L.; Ofori-Boateng, A.; Burns, J. L. Novel process for producing cubic liquid crystalline nanoparticles (cubosomes). *Langmuir* **2001**, *17*, 5748–5756.
- (23) Phan, S.; Fong, W.-K.; Kirby, N.; Hanley, T.; Boyd, B. J. Evaluating the link between self-assembled mesophase structure and drug release. *Int. J. Pharm.* **2011**, *421*, 176–182.
- (24) Wittkowski, R.; Löwen, H. Self-propelled Brownian spinning top: Dynamics of a biaxial swimmer at low Reynolds numbers. *Phys. Rev. E: Stat., Nonlinear, Soft Matter Phys.* **2012**, *85*, 021406.
- (25) de Campo, L.; Yaghmur, A.; Sagalowicz, L.; Leser, M. E.; Watzke, H.; Glatter, O. Reversible phase transitions in emulsified nanostructured lipid systems. *Langmuir* **2004**, *20*, 5254–5261.
- (26) Fong, W.-K.; Hanley, T.; Boyd, B. J. Stimuli responsive liquid crystals provide “on-demand” drug delivery in vitro and in vivo. *J. Controlled Release* **2009**, *135*, 218–226.
- (27) Fong, W.-K.; Hanley, T. L.; Thierry, B.; Tilley, A.; Kirby, N.; Waddington, L. J.; Boyd, B. J. Understanding the photothermal heating effect in non-lamellar liquid crystalline systems, and the design of new mixed lipid systems for photothermal on-demand drug delivery. *Phys. Chem. Chem. Phys.* **2014**, *16*, 24936–24953.
- (28) Yaghmur, A.; de Campo, L.; Sagalowicz, L.; Leser, M. E.; Glatter, O. Emulsified microemulsions and oil-containing liquid crystalline phases. *Langmuir* **2005**, *21*, 569–577.
- (29) Yaghmur, A.; de Campo, L.; Salentinig, S.; Sagalowicz, L.; Leser, M. E.; Glatter, O. Oil-Loaded Monolinolein-Based Particles with Confined Inverse Discontinuous Cubic Structure (Fd3m). *Langmuir* **2006**, *22*, 517–521.
- (30) Dong, Y.-D.; Larson, I.; Hanley, T.; Boyd, B. J. Bulk and dispersed aqueous phase behavior of phytantriol: effect of vitamin E acetate and F127 polymer on liquid crystal nanostructure. *Langmuir* **2006**, *22*, 9512–9518.
- (31) Tangso, K. J.; Patel, H.; Lindberg, S.; Hartley, P. G.; Knott, R.; Spicer, P. T.; Boyd, B. J. Controlling the Mesostructure Formation within the Shell of Novel Cubic/Hexagonal Phase Cetyltrimethylammonium Bromide–Poly(acrylamide-acrylic acid) Capsules for pH Stimulated Release. *ACS Appl. Mater. Interfaces* **2015**, *7*, 24501–24509.
- (32) Salentinig, S.; Sagalowicz, L.; Glatter, O. Self-Assembled Structures and pKaValue of Oleic Acid in Systems of Biological Relevance. *Langmuir* **2010**, *26*, 11670–11679.
- (33) Amar-Yuli, I.; Wachtel, E.; Shoshan, E. B.; Danino, D.; Aserin, A.; Garti, N. Hexosome and hexagonal phases mediated by hydration and polymeric stabilizer. *Langmuir* **2007**, *23*, 3637–3645.
- (34) Mezzenga, R.; Schurtenberger, P.; Burbidge, A.; Michel, M. Understanding foods as soft materials. *Nat. Mater.* **2005**, *4*, 729–740.
- (35) Rosa, M.; Rosa Infante, M.; Miguel, M. d. G.; Lindman, B. Spontaneous formation of vesicles and dispersed cubic and hexagonal particles in amino acid-based catanionic surfactant systems. *Langmuir* **2006**, *22*, 5588–5596.
- (36) Johnsson, M.; Lam, Y.; Barauskas, J.; Tiberg, F. Aqueous phase behavior and dispersed nanoparticles of diglycerol monoleate/glycerol dioleate mixtures. *Langmuir* **2005**, *21*, 5159–5165.
- (37) Neto, C.; Aloisi, G.; Baglioni, P.; Larsson, K. Imaging Soft Matter with the Atomic Force Microscope: Cubosomes and Hexosomes. *J. Phys. Chem. B* **1999**, *103*, 3896–3899.
- (38) Almgren, M.; Edwards, K.; Karlsson, G. Cryo transmission electron microscopy of liposomes and related structures. *Colloids Surf., A* **2000**, *174*, 3–21.
- (39) Boyd, B. J.; Rizwan, S. B.; Dong, Y.-D.; Hook, S.; Rades, T. Self-assembled geometric liquid-crystalline nanoparticles imaged in three dimensions: Hexosomes are not necessarily flat hexagonal prisms. *Langmuir* **2007**, *23*, 12461–12464.
- (40) Qi, J.; Nan, H.; Xu, D.; Cai, Q. Morphology Control of an MCM-41 Single Crystal with the Novel Hexagonal Circular Bicone Form. *Cryst. Growth Des.* **2011**, *11*, 910–915.
- (41) Jeong, J.; Davidson, Z. S.; Collings, P. J.; Lubensky, T. C.; Yodh, A. G. Chiral symmetry breaking and surface faceting in chromonic liquid crystal droplets with giant elastic anisotropy. *Proc. Natl. Acad. Sci. U.S.A.* **2014**, *111*, 1742–1747.
- (42) Lin, Z.; Liu, S.; Mao, W.; Tian, H.; Wang, N.; Zhang, N.; Tian, F.; Han, L.; Feng, X.; Mai, Y. Tunable Self-Assembly of Diblock Copolymers into Colloidal Particles with Triply Periodic Minimal Surfaces. *Angew. Chem., Int. Ed.* **2017**, *56*, 7135–7140.
- (43) Oka, T.; Ohta, N. Two Distinct Cylinder Arrangements in Monodomains of a Lyotropic Liquid Crystalline Hexagonal II Phase:

- Monodomains with Straight Cylinders and Ringed Cylinders in Capillaries. *Langmuir* **2016**, *32*, 7613–7620.
- (44) Boyd, B. Characterisation of drug release from cubosomes using the pressure ultrafiltration method. *Int. J. Pharm.* **2003**, *260*, 239–247.
- (45) Hong, L.; Salentinig, S.; Hawley, A.; Boyd, B. J. Understanding the mechanism of enzyme-induced formation of lyotropic liquid crystalline nanoparticles. *Langmuir* **2015**, *31*, 6933–6941.
- (46) Mulet, X.; Boyd, B. J.; Drummond, C. J. Advances in drug delivery and medical imaging using colloidal lyotropic liquid crystalline dispersions. *J. Colloid Interface Sci.* **2013**, *393*, 1–20.
- (47) Banquy, X.; Suarez, F.; Argaw, A.; Rabanel, J.-M.; Grutter, P.; Bouchard, J.-F.; Hildgen, P.; Giasson, S. Effect of mechanical properties of hydrogel nanoparticles on macrophage cell uptake. *Soft Matter* **2009**, *5*, 3984.
- (48) Kersey, F. R.; Merkel, T. J.; Perry, J. L.; Napier, M. E.; DeSimone, J. M. Effect of Aspect Ratio and Deformability on Nanoparticle Extravasation through Nanopores. *Langmuir* **2012**, *28*, 8773–8781.
- (49) Merkel, T. J.; Jones, S. W.; Herlihy, K. P.; Kersey, F. R.; Shields, A. R.; Napier, M.; Luft, J. C.; Wu, H.; Zamboni, W. C.; Wang, A. Z.; Bear, J. E.; DeSimone, J. M. Using mechanobiological mimicry of red blood cells to extend circulation times of hydrogel microparticles. *Proceedings of the National Academy of Sciences* **2011**, *108*, 586–591.
- (50) Salo-Väänänen, P.; Ollilainen, V.; Mattila, P.; Lehikoinen, K.; Salmela-Mölsä, E.; Piironen, V. Simultaneous HPLC analysis of fat-soluble vitamins in selected animal products after small-scale extraction. *Food Chem.* **2000**, *71*, 535–543.
- (51) Schneider, C. A.; Rasband, W. S.; Eliceiri, K. W. NIH Image to ImageJ: 25 years of image analysis. *Nat. Methods* **2012**, *9*, 671–675.
- (52) Dierking, I. *Textures of Liquid Crystals*; John Wiley & Sons, 2003.
- (53) Rosevear, F. B. The microscopy of the liquid crystalline neat and middle phases of soaps and synthetic detergents. *J. Am. Oil Chem. Soc.* **1954**, *31*, 628–639.
- (54) Livolant, F.; Bouligand, Y. Liquid crystalline phases given by helical biological polymers (DNA, PBLG and xanthan). Columnar textures. *J. Phys.* **1986**, *47*, 1813–1827.
- (55) Kirby, N. M.; Mudie, S. T.; Hawley, A. M.; Cookson, D. J.; Mertens, H. D. T.; Cowieson, N.; Samardzic-Boban, V. A low-background-intensity focusing small-angle X-ray scattering undulator beamline. *J. Appl. Crystallogr.* **2013**, *46*, 1670–1680.
- (56) Mudie, S. Scatterbrain Software. www.synchrotron.org.au, 2017.
- (57) Soni, S. S.; Brotons, G.; Bellour, M.; Narayanan, T.; Gibaud, A. Quantitative SAXS analysis of the P123/water/ethanol ternary phase diagram. *J. Phys. Chem. B* **2006**, *110*, 15157–15165.
- (58) Wood, E. A. *Crystals and light: an introduction to optical crystallography*; Courier Corporation, 1977.
- (59) Martiel, I.; Sagalowicz, L.; Handschin, S.; Mezzenga, R. Facile dispersion and control of internal structure in lyotropic liquid crystalline particles by auxiliary solvent evaporation. *Langmuir* **2014**, *30*, 14452–14459.
- (60) Warren, P. B.; Prinsen, P.; Michels, M. A. J. The physics of surfactant dissolution. *Philos. Trans. R. Soc., A* **2003**, *361*, 665–676.
- (61) Shearman, G. C.; Ces, O.; Templer, R. H.; Seddon, J. M. Inverse lyotropic phases of lipids and membrane curvature. *J. Phys.: Condens. Matter* **2006**, *18*, S1105–S1124.
- (62) Tran, N.; Mulet, X.; Hawley, A. M.; Conn, C. E.; Zhai, J.; Waddington, L. J.; Drummond, C. J. First direct observation of stable internally ordered Janus nanoparticles created by lipid self-assembly. *Nano Lett.* **2015**, *15*, 4229–4233.
- (63) Sagalowicz, L.; Guillot, S.; Acquistapace, S.; Schmitt, B.; Maurer, M.; Yaghmur, A.; de Campo, L.; Rouvet, M.; Leser, M.; Glatter, O. Influence of vitamin E acetate and other lipids on the phase behavior of mesophases based on unsaturated monoglycerides. *Langmuir* **2013**, *29*, 8222–8232.
- (64) Amar-Yuli, I.; Wachtel, E.; Shalev, D. E.; Aserin, A.; Garti, N. Low viscosity reversed hexagonal mesophases induced by hydrophilic additives. *J. Phys. Chem. B* **2008**, *112*, 3971–3982.
- (65) Pawar, A. B.; Caggioni, M.; Hartel, R. W.; Spicer, P. T. Arrested coalescence of viscoelastic droplets with internal microstructure. *Faraday Discuss.* **2012**, *158*, 341–350.
- (66) Caggioni, M.; Bayles, A. V.; Lenis, J.; Furst, E. M.; Spicer, P. T. Interfacial stability and shape change of anisotropic endoskeleton droplets. *Soft Matter* **2014**, *10*, 7647–7652.
- (67) Seddon, J. M. Structure of the inverted hexagonal (HII) phase, and non-lamellar phase transitions of lipids. *Biochim. Biophys. Acta, Biomembr.* **1990**, *1031*, 1–69.
- (68) Guttman, S.; Sapir, Z.; Ocko, B. M.; Deutsch, M.; Sloutskin, E. Temperature-tuned faceting and shape changes in liquid alkane droplets. *Langmuir* **2017**, *33*, 1305–1314.
- (69) Lynch, M. L.; Kochvar, K. A.; Burns, J. L.; Laughlin, R. G. Aqueous-Phase Behavior and Cubic Phase-Containing Emulsions in the C12E2–Water System. *Langmuir* **2000**, *16*, 3537–3542.
- (70) Pieranski, P.; Bouchih, M.; Ginestet, N.; Popa-Nita, S. Concave and convex shapes of the Pn3m/L1 interface. *Eur. Phys. J. E: Soft Matter Biol. Phys.* **2003**, *12*, 239–254.
- (71) Latypova, L.; Góźdź, W.; Pieranski, P. Symmetry, topology and faceting in bicontinuous lyotropic crystals. *Eur. Phys. J. E: Soft Matter Biol. Phys.* **2013**, *36*, 88.
- (72) Malkin, A. J.; Kuznetsov, Y. G.; McPherson, A. In situ atomic force microscopy studies of surface morphology, growth kinetics, defect structure and dissolution in macromolecular crystallization. *J. Cryst. Growth* **1999**, *196*, 471–488.
- (73) Clark, J. N.; Ihli, J.; Schenk, A. S.; Kim, Y.-Y.; Kulak, A. N.; Campbell, J. M.; Nisbet, G.; Meldrum, F. C.; Robinson, I. K. Three-dimensional imaging of dislocation propagation during crystal growth and dissolution. *Nat. Mater.* **2015**, *14*, 780–784.
- (74) Impérator-Clerc, M.; Davidson, P. An X-ray scattering study of flow-aligned samples of a lyotropic liquid-crystalline hexagonal phase. *Eur. Phys. J. B* **1999**, *9*, 93–104.
- (75) Oswald, P.; Géminard, J. C.; Lejcek, L.; Sallen, L. Nonlinear analysis of stripe textures in hexagonal lyotropic mesophases. *J. Phys. II* **1996**, *6*, 281–303.
- (76) Zhang, R.; Zeng, X.; Kim, B.; Bushby, R. J.; Shin, K.; Baker, P. J.; Percec, V.; Leowanawat, P.; Ungar, G. Columnar liquid crystals in cylindrical nanoconfinement. *ACS Nano* **2015**, *9*, 1759–1766.
- (77) Kleman, M. Developable domains in hexagonal liquid crystals. *J. Phys.* **1980**, *41*, 737–745.
- (78) Damasceno, P. F.; Engel, M.; Glotzer, S. C. Predictive Self-Assembly of Polyhedra into Complex Structures. *Science* **2012**, *337*, 453–457.